Ivanov, Valentin :

Analysis of Tire Contact Parameters Using Visual Processing

Zuerst erschienen in:
Advances in tribology. - New York, NY : Hindawi. - 2010, Article ID 491723, insges. 11 S.
DOI: 10.1155/2010/491723

Hindawi Publishing Corporation
Advances in Tribology
Volume 2010, Article ID 491723, 11 pages
doi:10.1155/2010/491723

Research Article

Analysis of Tire Contact Parameters Using Visual Processing

Valentin Ivanov

Automotive Engineering Department, Ilmenau University of Technology, Gustav-Kirchhoff-Platz 2, 98693 Ilmenau, Germany

Correspondence should be addressed to Valentin Ivanov, valentin.ivanov@tu-ilmenau.de

Received 16 January 2010; Revised 3 May 2010; Accepted 6 May 2010

Academic Editor: Qian Wang

This paper discusses the application of noncontact methods to analyze the tire-surface contact interaction. This approach uses the tire test bench with the set of contact patch monitoring based on image processing procedures. The first part of this paper presents the results of experimental estimation of the contact patch area depending on the normal wheel load and inflation pressure for different car tires. The data were obtained for test bench conditions on the basis of the visual processing of tread footprint. Further, the contact length in the cohesion area during wheel rolling for single points on the tire profile has been chosen as a benchmark criterion. This paper has analyzed the influence of the wheel normal load and tire inflation pressure on the contact length with small rolling velocities. The results of the investigations are given for winter and racing tires with different grades of wear.

1. Introduction

The permanent development of new methods in simulation and experimental research on contact processes of tire-surface interaction furnishes an opportunity to perfect both the tire construction and the automotive control systems considering the wheel dynamics. Nevertheless, the complicated mathematical apparatus describing the tire contact processes, which is typical for many up-to-date research works, does not always allow easy-to-use assessment of such fundamental parameters as contact patch area or pneumatic trail.

The mentioned parameters are of importance for a comparative analysis of tire construction, especially for

(i) approbation of new tread materials,

(ii) assessment of tread pattern impact on tire kinematic,

(iii) verification of model validity in respect of tire-road interaction.

An analysis of related research sources has revealed that the following theoretical methods are most commonly used for assessing tire contact characteristics:

(i) multi-body models [1–3],

(ii) tribological models [4],

(iii) finite element analysis [5, 6],

(iv) inverse dynamics, observers [7–9].

To parameterize and verify the tire contact models, field and rig testing can be applied. For this, the methods of thermograph, optical, and acoustical measurements have received recognition [10–13], or the typical tribological measurements can be applied to tire specimens [14].

Within the framework of this paper, another approach is considered. It is based on a combination of a nondestructive measuring technique and visual information processing. Two case studies are further discussed to illustrate the applicability of the proposed method for the analysis of contact patch area and contact length. This paper advances the results obtained by the author and published in [16, 17].

2. Test Equipment

The data for analysis of tire contact properties, which will be examined in the next sections, were obtained using the tire test rig [15] shown in Figures 1 and 2 with the technical data indicated in Table 1. This construction allows mounting a tire on axial bearing with the possibility of adjusting the vertical loading, the turning angle on the tangential plane, and the inclination angle on the vertical plane. The rotation of the tire evolves from the movement of the bearing plate from

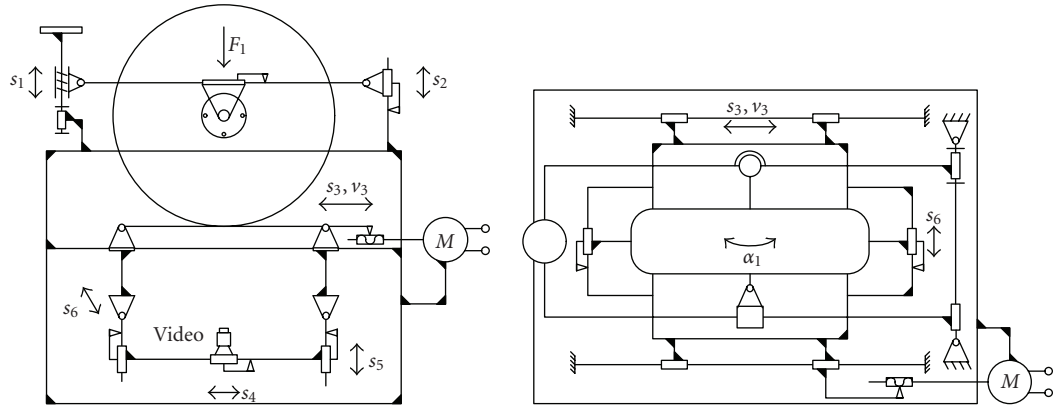

(a) (b)

Figure 1: Schema of tire test rig [15].

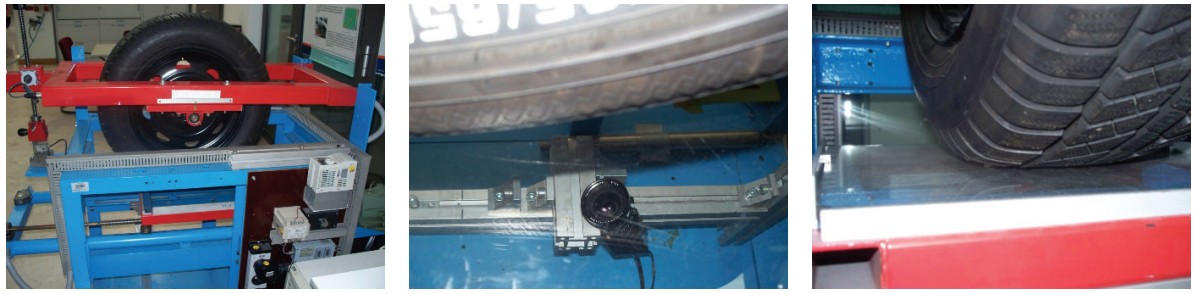

(a) (b) (c)

Figure 2: Test rig view.

Table 1: Technical data of tire test rig.

Functional parameter	Value
Tire turning angle α_1 (°)	$-5 \cdots +5$
Vertical loading F_1 (N)	$0 \cdots 6000$
Height of loading device installation s_1 (mm)	≤ 100
Measurement range of vertical deformation s_2 (mm)	$0 \cdots 150$
Tangential displacement of bearing plate s_3 (mm)	$0 \cdots 600$
Tangential displacement of video camera s_4 (mm)	$0 \cdots 500$
Vertical displacement of video camera s_5 (mm)	$0 \cdots 400$
Displacement for camera's inclination s_6 (mm)	$0 \cdots 200$
Maximal speed of plate movement v_3 (m/s)	0.03
Diameter of tested tire (mm)	$400 \cdots 650$
Maximal width of tested tire (mm)	380

armored glass. The drive electric motor controls the velocity of the plate movement. A video camera with CCD-matrix is placed under the glass plate and provides a shooting speed of 30 frames per second. Using the camera, snapshots of the contact patches were obtained, and National Instruments Vision Assistant [18] software was used to process these pictures.

The procedure of testing can be briefly presented through the following milestones.

(1) *Calibration of Video-Measuring System*. For this purpose the video camera takes a picture of a grid with cells of 10×10 mm and nodes with diameter of 1 mm, Figure 3(a). This picture is saved in memory as a reference template.

(2) Depending on measurement task, the camera shoots either single picture of contact patch by predetermined tire inflation and loading (case 1, Figure 3(b)) or sequence of pictures during the tire rolling (case 2, Figure 3(d)).

(3) *For Case* 1. Using internal algorithm of National Instruments Vision Assistant software, the picture of contact patch transformed to a pattern allowing subsequent numerical processing, Figure 3(c). Then the actual area of this pattern is recalculated using reference template from pixels to square units (mm^2). It should be mentioned that there is a possibility to compute both whole contact area and nominal contact area. As applied to Figure 3(c), nominal contact area covers only "black" objects; all "white" pixels are excluded from processing.

(4) *For Case* 2. Sequence of pictures can be used to trace positions of singular tire points during their movement within contact area. For this purpose, National Instruments Vision Assistant software measures for

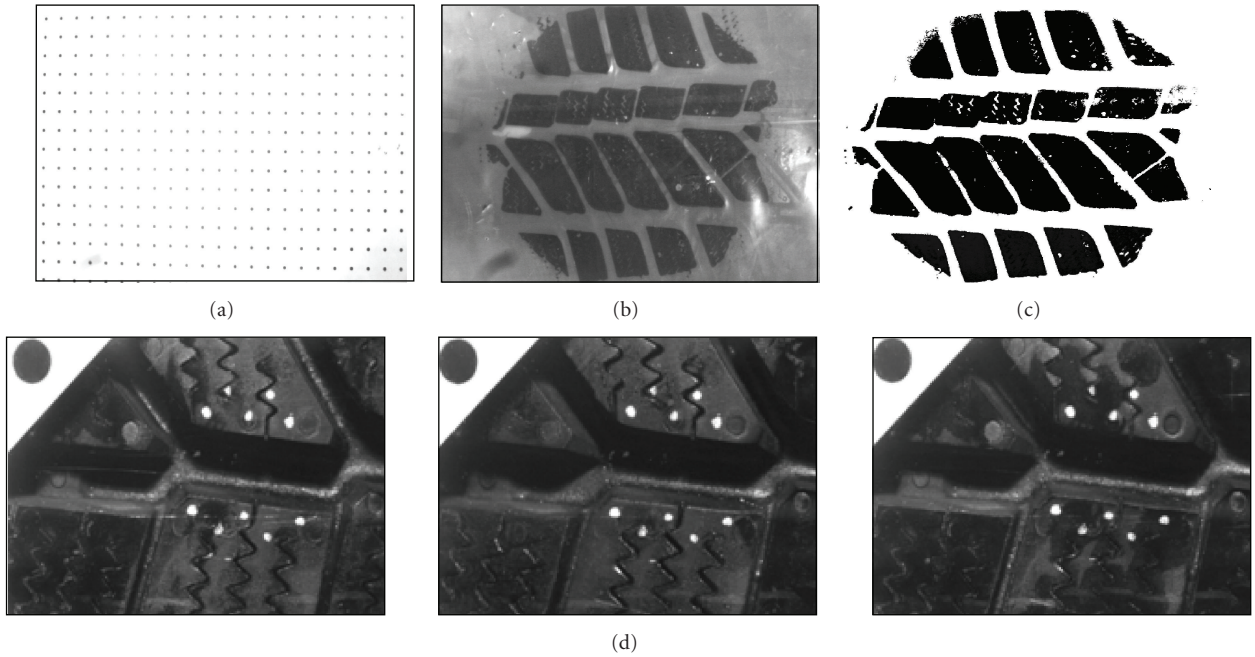

Figure 3: Examples of snapshots illustrating the test procedure.

every picture in sequence the distance between certain reference stationary point and moving tire point. During experiments, the sequences have been made with frequency up to 10 snapshots per second. More detailed description of this procedure will be given in next paper sections.

3. Case Study 1: Contact Patch Area

3.1. Theoretical Background. The area of tire/surface contact is the crucial parameter in analyzing the influence of various surface and vehicle parameters on contact friction processes. It should distinguish between the tire contact area and the nominal touch patch because of the tread pattern. In this connection the following formula is used for the calculation:

$$A_c = k_s \cdot A_f, \tag{1}$$

where A_f is the full area of tire contact region, A_c is the nominal contact area, and k_s is the coefficient of tread pattern saturation. Here the nominal contact area does not take into consideration the microtexture of contacting surfaces.

The pressures on single points within the contact patch differ in value depending on many operational parameters, and therefore the average factors are reasonable for the initial assessment of contact interaction:

(i) mean contour pressure within the contact area is given as

$$p_m = \frac{F_z}{A_f}, \tag{2}$$

(ii) average stress is given as

$$p_c = \frac{F_z}{A_c}, \tag{3}$$

(iii) coefficient of tread loading equilibrium is given as

$$k_t = \frac{p_c}{p}, \tag{4}$$

where F_z is normal wheel load and p is tire inflation pressure.

3.2. Tire Specimens and Test Program. To find possible regularities in forming the tire contact area, five tires from different manufacturers with diverse tread patterns were chosen as testing objects:

(i) Tire 1: 155/70 R13 75S (used),

(ii) Tire 2: 195/65R15 91H (used),

(iii) Tire 3: 185/65R14 86T (new),

(iv) Tire 4: 175/70R13 82H (used),

(v) Tire 5: 155/70R13 78S (used).

Figure 4 shows how the contact patch can be visually presented on the discussed test rig with corresponding software. It should be pointed out that the representation of contact area in a three-dimensional form is obtained using special procedures of National Instruments Vision Assistant software. These procedures estimate brightness, intensity, and contrast of the snapshot and reconstruct the 3D object. This transformation serves an illustrative purpose. In addition, Figure 5 gives examples of treated pictures

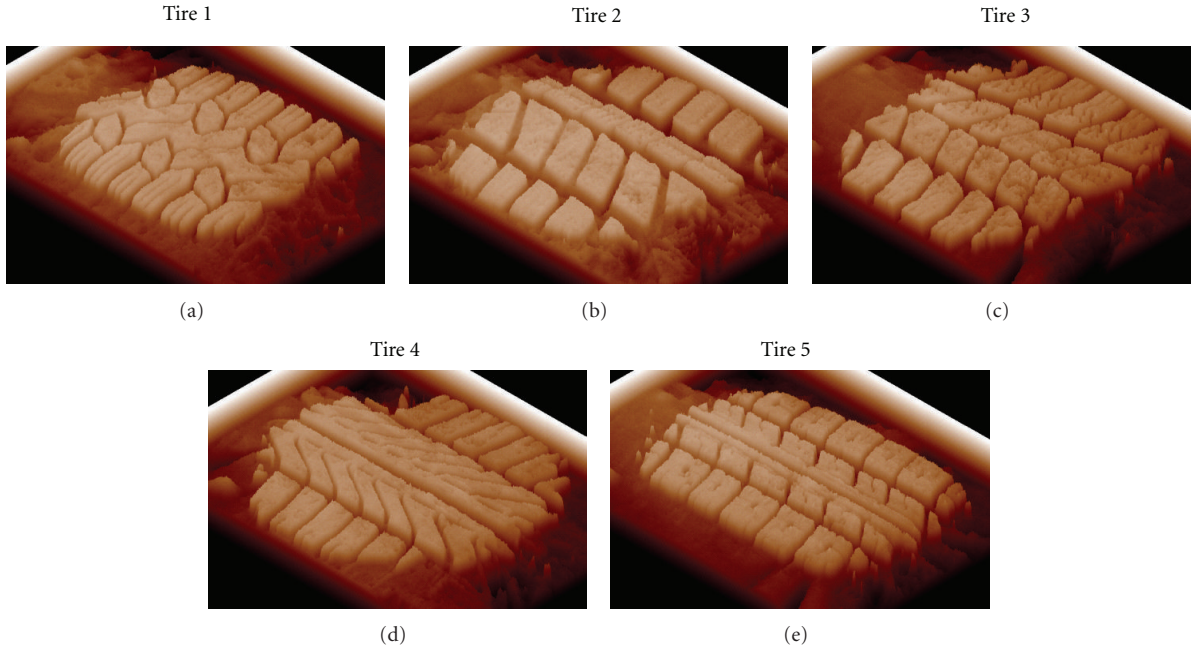

Figure 4: 3D contact patches.

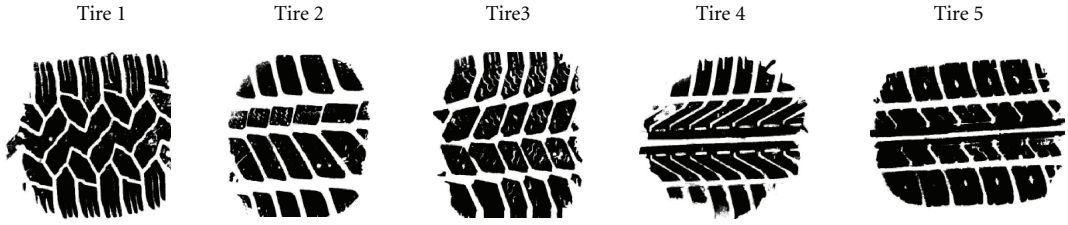

Figure 5: Examples of processed contact patches.

suitable for subsequent numerical processing of the tire contact area.

The test program was similar for each of the tires under investigation and consisted of visual processing of contact patches under the following conditions:

(i) Tire inflation pressure p: 1.8 bar, 2.1 bar, 2.4 bar, 2.7 bar,

(ii) Normal wheel load F_z: 1000 N, 1500 N, 2000 N, 3000 N, 4000 N.

3.3. Discussion of Test Results for Contact Patch Area

3.3.1. Tread Pattern Saturation. Table 2 shows the statistical data for coefficient k_s for the tires under investigation based on all ranges of changeable parameters (tire inflation pressure and wheel loading). It may be noted that for this parameter the tire inflation pressure and wheel load have insignificant influence on the magnitude of the coefficient of tread pattern saturation. Moreover, the coefficients k_s from (1) lie within the narrow limits for all tested tires. These observations are evidence of unused potential in the development of treads with variable patterns that may allow enhancement of the design of tires with adaptive properties.

Table 2: Coefficients of tread pattern saturation.

	Mean value	Minimal value	Maximal value	Standard deviation
Tire 1	0.6062	0.5602	0.6700	0.0297
Tire 2	0.5374	0.4863	0.5736	0.0221
Tire 3	0.6028	0.5381	0.6969	0.0431
Tire 4	0.5573	0.5124	0.6006	0.0215
Tire 5	0.5916	0.4516	0.6652	0.0469

3.3.2. Nominal Contact Area. The normal wheel load influences the nominal contact area A_c; the tire inflation pressure has an effect to a lesser extent. The value of A_c is directly proportional to F_z and is inversely proportional to p. Figure 6 displays the characteristic dependencies for the tire 195/65R15 91H (Tire 2). It should be mentioned that a fourfold difference can take place between the nominal contact areas within the range of operational pressures and loads. From this point on, the approximate statistical dependencies are within a confidence interval of 95%.

In Figure 7 the functions $A_c = f(p)$ for a complete range of load $F_z = 1000 \cdots 4000$ N are compared for all the tires.

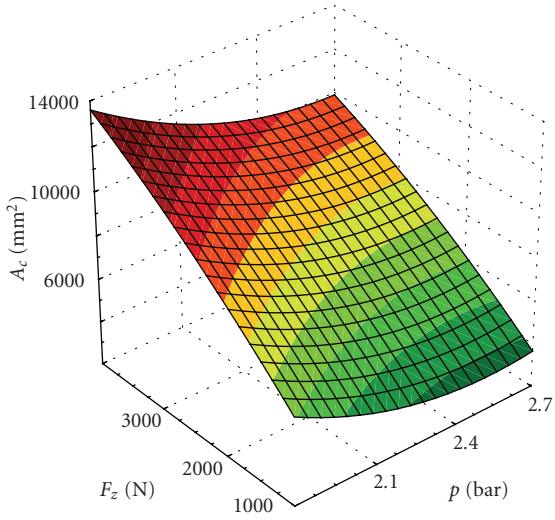

Figure 6: Nominal contact area for Tire 2 as a function of pressure and vertical load.

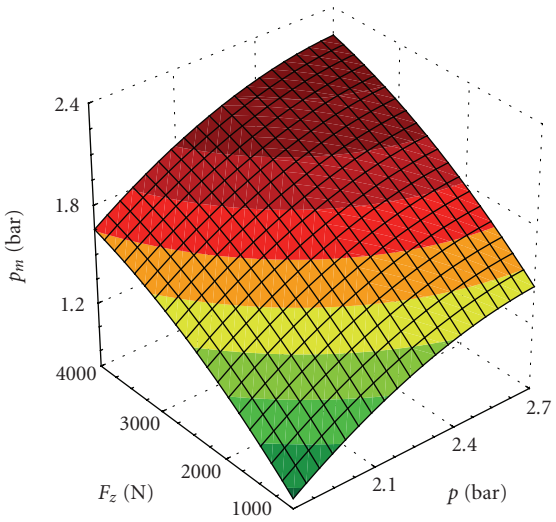

Figure 8: Average contour pressure for Tire 2 as a function of pressure and vertical load.

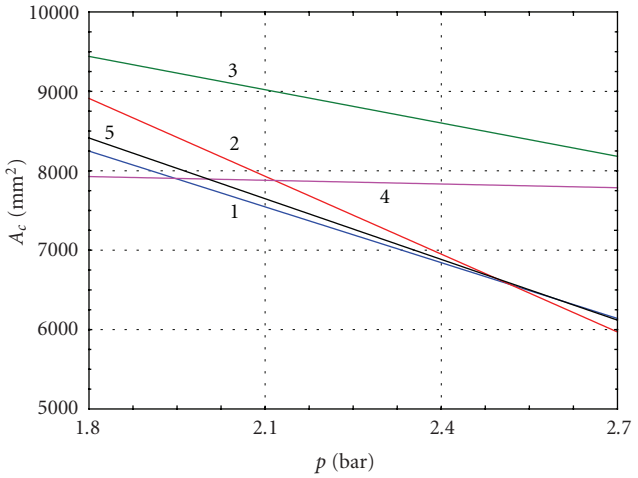

Figure 7: Mean values of contact areas (for total range of normal load) as a function of pressure.

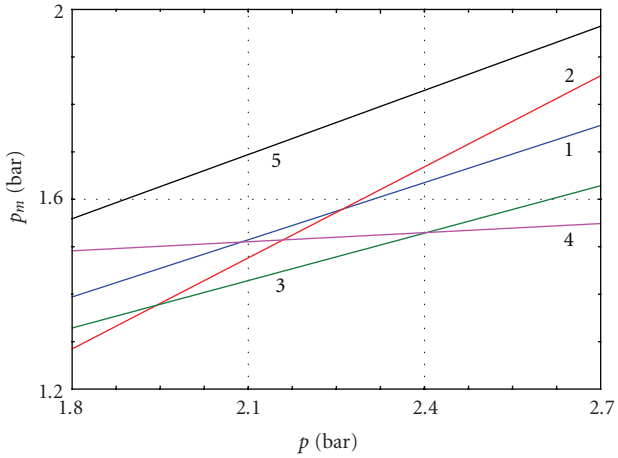

Figure 9: Average contour pressure (for total range of normal load) as a function of pressure.

The analysis of these diagrams indicates that even tires of the same class, which have close chemical compositions of rubber and friction properties, can offer completely different contact characteristics in plane. Disregard of this factor can lead to serious inaccuracy in the tire models especially in research on curvilinear and vertical vehicle dynamics when the tire contact area has an essential impact on forming the wheel forces and moments.

3.3.3. Average Contour Pressure. The average contour pressure p_m estimates virtually the load transfer from a vehicle to a road through a tire. This parameter is mainly used to form the loading modes of roadway. An example of characteristics for the tire 195/65R15 91H (Tire 2), presented in Figure 8, shows that the equivalent average stress is always less than the tire inflation pressure. The comparative analysis of the regression lines $p_m = f(p)$ for five tires has revealed only a different character for Tires 3 and 4. Other tires had similar behavior of the parameter p_m in dependence on the wheel load (Figure 9). The difference in characteristics for various tires can be explained in the first place by diverse tread patterns. This effect is now under further investigations.

3.3.4. Coefficient of Tread Loading Equilibrium. Considering the toroidal tire model, the coefficient of tread loading equilibrium k_t allows assessment of loading modes for tread as a shell. Furthermore, this parameter is useful during investigations of internal friction in the tread elements as it reflects the balance between the deformation loading of an element both from the surface and from the tire inflation pressure. Figure 10 shows the functions $k_t = f(p, F_z)$ for Tire 2. These curves for other tires under discussion have similar shapes and they can be described by the polynomial 3D functions.

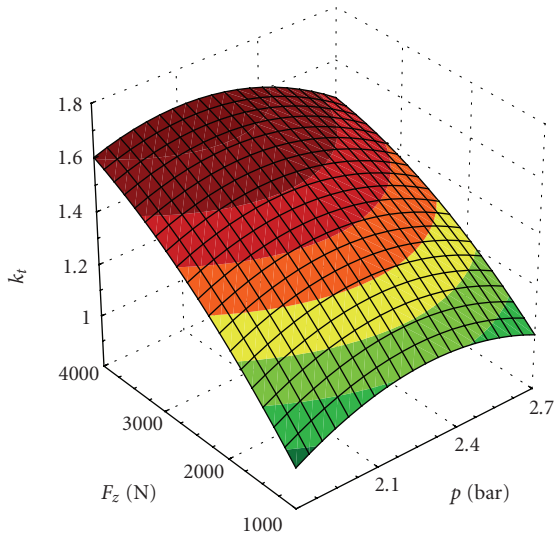

FIGURE 10: Coefficient of tread loading equilibrium for Tire 2 as a function of pressure and vertical load.

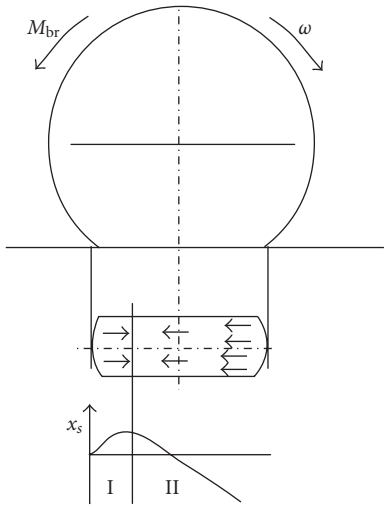

FIGURE 11: Tire rolling during braking. I: slipping region; II: adhesion region; x_s: friction contact length.

4. Case Study 2: Pneumatic Trail

4.1. Theoretical Background. It is common practice to subdivide the tire-surface contact into the cohesion and slipping areas on a global scale (Figure 11). It is assumed that two areas arise within the tire patch where the tire tread is either shrinking (before contact) or stretching (after contact). Therefore the vehicle velocity applied to the wheel centre v does not correspond to the wheel circumferential velocity $\omega \cdot r$ in a contact area, where ω is the wheel's angular velocity and r is the dynamic tire radius. It is because of this fact that in the immediate region of the contact patch the slipping occurs, that is, the shift of rubber elements due to which the tangential stresses exceed the specific tangential and lateral forces. For example, the mentioned tangential stresses τ_x

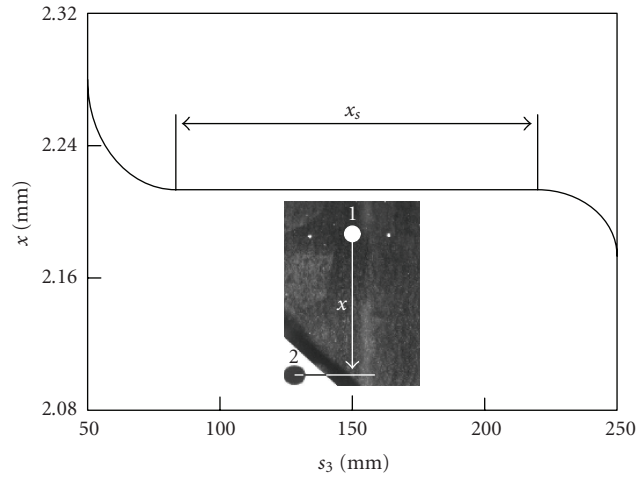

FIGURE 12: The observation of contact length. s_3: tangential displacement of bearing plate (see Figure 1).

at braking can be separated into the following components [19]:

$$\tau_x = \tau_d + \tau_r + \tau_v - \Delta\tau_{\text{br}}, \tag{5}$$

where component τ_d is due to the tire macrodeformation from the normal loading; component τ_r is caused by the wheel rolling resistance; component τ_v is due to the difference between the rotation frequencies of tread elements within the contact and out of this area; and $\Delta\tau_{\text{br}}$ is motivated from the brake moment.

The qualitative comparison of contact properties through the deformation components for the different tires is highly conjectural, since the distribution law for the components τ_d, τ_v, and $\Delta\tau_{\text{br}}$ is commonly gleaned from the empirical base depending on the contact patch size.

The force within contact is the effort expended on destruction of frictional ties at cohesion. From here its potential character will be obvious; that is, in order for a slipping contact between a motioning wheel and a surface to appear, the contact forces should have cohesion potential. Hence, at the moment of the slip beginning the tire cohesion force should lie in one interval limited by many factors: loading, temperature, surface conditions, tire inflation pressure, and so on. One of the variants of comparative tire analysis regarding the potential parameters is based on the characteristics obtained for the driven mode of wheel rolling. As applied to this matter, the problems of experimental investigations are discussed next.

4.2. Test Program. Using the test rig and visual processing software under consideration, the following testing procedures for the assessment of contact length (length of cohesion area or pneumatic trail) were performed.

The driven mode of wheel rolling was initially chosen for the test conditions. In vehicle dynamics, the driven mode implies that a tire has no torque applied directly to its axle and moves only through the reduced propelling force. In contrast, a torque is always applied during the driving mode.

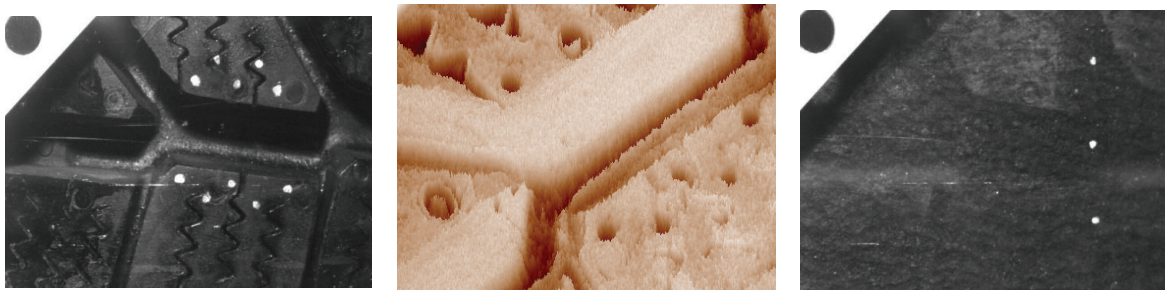

(a) (b) (c)

Figure 13: Tire surfaces under tests: (a) observed points on tread elements; (b) 3D handling and magnification of tread elements; (c) observed points on slick tire.

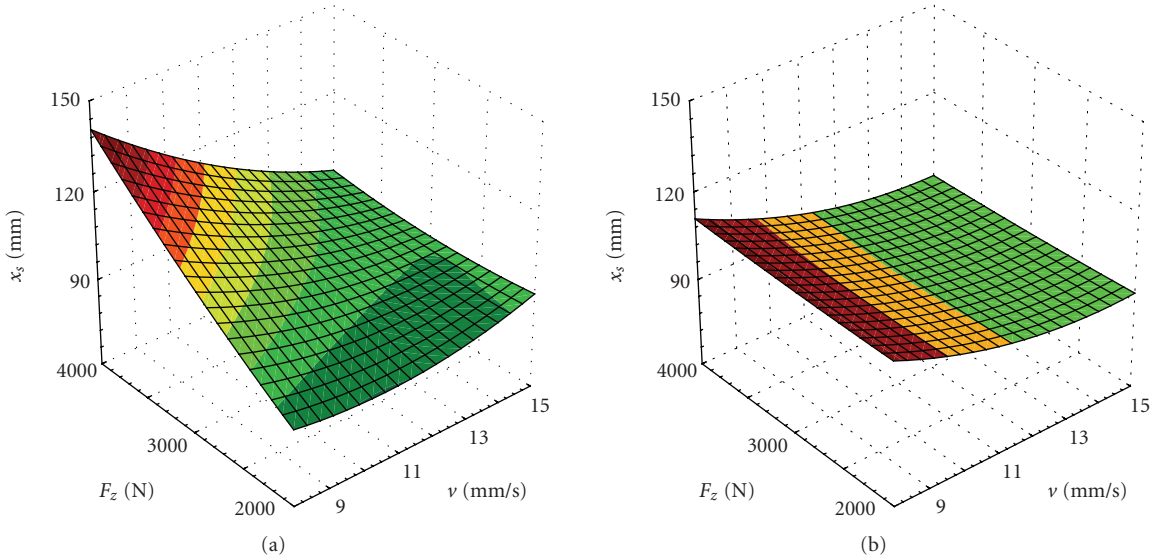

Figure 14: Cohesion contact length of rolling tire in a driven mode: (a) for upper tread element from Figure 13(a); (b) for lower tread element from Figure 13(a).

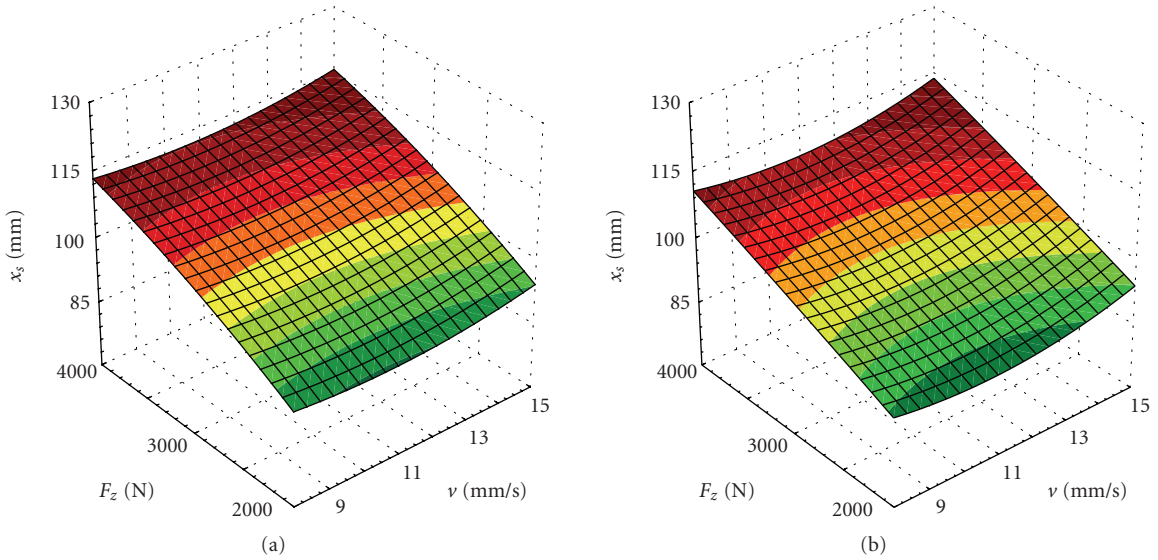

Figure 15: Cohesion contact length of rolling tire in braking mode: (a) for upper tread element from Figure 13(a) ; (b) for lower tread element from Figure 13(a).

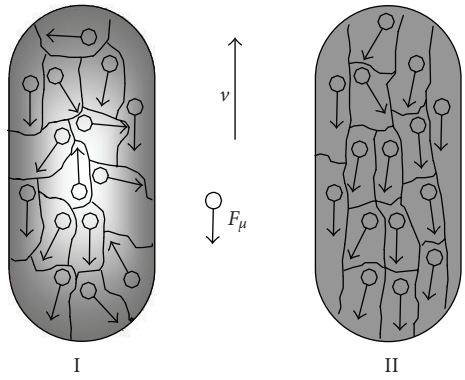

Figure 16: The localization of tire contact forces. I: rolling in driven mode; II: rolling in braking mode; v: velocity; F_μ: local maximal friction force.

The slipping processes within the contact patch are of a minor nature for driven mode in comparison with braking or driving. This gives an opportunity to determine the actual nonslip contact length including the length for a single point in the tire contact. Relative to the slipping velocity or coefficient of wheel slip, this parameter is more reliable for the comparative tire analysis with respect to the deformation parameters as well as for investigations of the influence of external factors on the contact patch. Figure 12 illustrates the determination of the mentioned variable.

In accordance with Figure 12, the video camera traces the pattern within which the displacement of a certain point 1 on the tire surface can be followed relative to the fixed point 2 on the plate surface. Through the wheel rolling process, point 1, coming into the contact patch area, ceases the relative movement during the interval x_s and is shifted only together with the bearing plate due to the so-called "sticking" effect. The distance x_s corresponds to the actual contact length without slipping. Hence the experimental task was to get the parameter x_s for various tires under the different loading conditions.

The tested specimens are

(i) winter tire 195/65 R 15 91H with skew profile (Tire 2 from Case Study 1),

(ii) racing tire without tread pattern ("slick tire") 16/55-13.

The experiments were performed in the following order.

(1) *Test 1*. Winter tire; glass plate surface. Measurements for 10 points on two different tread elements; Figures 13(a) and 13(b).

(2) *Test 2*. Winter tire; glass plate surface. Measurements for two different tread elements on applying the brake moment to the wheel. The braking power was equivalent to up to 30% of the driving motor power. This test was performed for a qualitative analysis of contact processes with the wheel rolling in the driven and braking modes.

(3) *Test 3*. Slick tire with new tread; glass plate surface. Measurements for three points placed on one crosscut line relative to the direction of movement; Figure 13(c).

(4) *Test 4*. Slick tire with worn tread; glass plate surface. Measurements for three points placed on one crosscut line relative to the direction of movement. The tread wear lies within the limits allowing further tire running.

The following operational parameters have been varied during the experiments:

(i) speed of plate movement v_3 (see Figure 1): 8.4 mm/s, 11.2 mm/s, 14.0 mm/s,

(ii) tire inflation pressure p: 1.2 bar, 1.8 bar, 2.4 bar,

(iii) vertical loading F_z: 2000 N, 3000 N, 4000 N.

The number of measurements is three samples for each of the parameter combinations "tire inflation: wheel loading: velocity", which is equivalent to 81 samples for every point on the tire tread. For this, an equivalent uncertainty of visual processing was no more than 0.085 mm. Functional dependencies for test results have been obtained by means of statistical treatment through third-order polynomial approximation with a confidence interval of 95%.

4.3. Discussion of Test Results for Pneumatic Trail

4.3.1. Winter Tire. Figure 14 shows examples of treated experimental dependencies for rolling the winter tire in a driven mode. In this picture the contact length x_s for two neighboring tread elements is displayed as a function of vertical loading F_z and contact velocity v for the total range of inflation pressure $p = 1.2$–2.4 bar.

The test results allowed the following conclusions to be drawn.

(1) Under the testing conditions the contact length for a driven mode of wheel rolling increases proportionately to the increase in normal wheel loading irrespective of the tire inflation pressure.

(2) With fixed wheel loading and tire pressure, the contact length depends moderately on the velocity.

(3) The difference in the contact lengths for two random points on the tire surface can be up to 15%–20% for all modes of performed tests, even for the same tread elements. This conclusion is of fundamental importance since it allows the contact processes due to tire rolling to be considered as objects of the uncertain dynamics.

The tests of a braking wheel were performed for a qualitative assessment with a fixed magnitude of the brake moment. The corresponding dependencies, as for a driven mode, are shown in Figure 15.

This experiment allowed the following conclusions to be drawn.

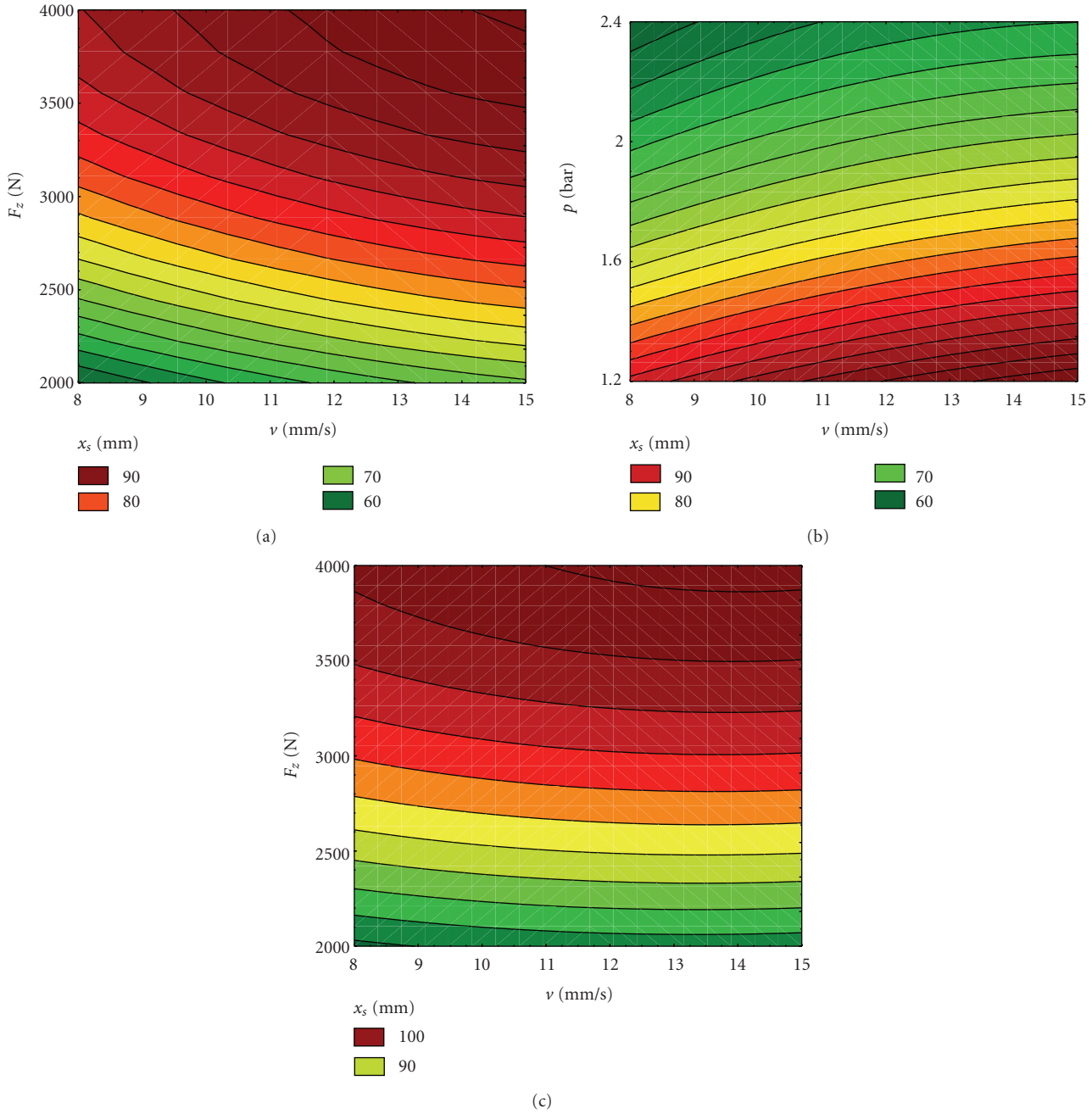

FIGURE 17: Examples of regression characteristics of cohesion contact length for the rolling of a slick tire in a driven mode: (a) new tire with $p = 2.1$ bar = const; (b) new tire with $F_z = 4000$ N = const; (c) worn tire with $p = 2.1$ bar = const (from [16]).

(1) Under fixed pressure and wheel loading the contact length does not depend practically on the rolling velocity.

(2) As for the driven mode, the increase in tire inflation pressure reduces the contact length.

(3) In comparison with the driven mode, the increase in the normal loading leads to an increase in contact to only a small extent.

(4) The average values of the cohesion contact length differ insignificantly between the braking and driven modes (because the brake test corresponded to partial braking without wheel blocking). But the parameter range for the single points within the contact of the tread elements was minor for braking: 0.5%–7% on average.

The last conclusion confirms the hypothesis about the localization of the maximal friction forces within tire-road contact (Figure 16) [20]. At any rolling of elastic pneumatic the local use of the maximal friction force of the tire-road interaction F_μ takes place because of the kinematic

Table 3: The contact lengths for the slick tire rolling in a driven mode for the interval of normal loading $F_z = 2000 \cdots 4000$ N (from [16]).

New tire-glass plate surface			
x_s (mm)		v (mm/s)	
	8.4	11.2	14.0
$p = 1.2$ bar	64.4–106.4	67.2–109.5	70.0–112.0
$p = 1.8$ bar	50.4–86.8	63.5–89.6	60.7–88.7
$p = 2.4$ bar	50.4–72.8	48.5–70.9	56.0–74.7
Worn tire-glass plate surface			
x_s (mm)		v (mm/s)	
	8.4	11.2	14.0
$p = 1.2$ bar	92.4–112.0	97.1–112.0	102.7–116.0
$p = 1.8$ bar	78.4–109.2	78.4–104.5	67.2–112.0
$p = 2.4$ bar	64.4–98.0	67.2–97.1	65.3–98.0

misalignment between the tire profile and the road surface. The grade of this localization depends on the intensity of applied driving or braking torque.

4.3.2. Slick Tire. Because the functional purpose of the slicks is limited only by the application on high-speed racing cars, the chemical composition and structure of such tires differs essentially from the parameters of conventional tires. For the research tasks in hand the lack of the tread pattern on slicks is of great importance since the tread geometry does not impact on the contact length in this case, and there is a possibility of data gathering for the rolling of an "idealized" tire. Table 3 shows the test results for slick tire. Figure 17 gives examples of the obtained dependencies.

Here the following conclusions can be drawn.

(1) The results of slick tire rolling on the glass surface verify that the contact length increases significantly with the tread wearing.

(2) It was indicated that the influence of the wheel loading and tire inflation pressure on the contact length has a monotonous proportional character, as contrasted with the tires with tread patterns.

(3) The dispersion of values for single contact points is essentially lower than for the winter tire and is no more than 8%–10%. This effect of stable characteristics can be caused by minor influence of the internal tire rubber for the slick tires.

5. Summary and Conclusions

The performed investigations illustrated a good possibility for the application of noninvasive methods and visual processing to the quantitative assessment of tire contact interaction. As applied to the contact patch area, the proposed procedures allow estimation of the tread pattern saturation, real contact area, average contact strain, and coefficient of tread loading equilibrium. The corresponding test results were illustrated in the paper for five different car tires. A pneumatic trail is the next discussed parameter that can be assessed with the proposed visual processing method. The experimental data for winter tires and slick tires have allowed a comparative analysis to be made for the cohesion contact length in various operational modes.

The author plans to discuss the application of the described methods to the analytical issues of tire dynamics in future works.

Acknowledgments

This paper was started with the support of Alexander von Humboldt Foundation (test data gaining) and has been further processed and advanced as initial part of a Marie Curie—International Incoming Fellowship—project "INTYRE" within the 7th European Community Framework Programme. The author would like to thank Prof. Dr.-Ing. Klaus Augsburg and DiplEng. Barys Shyrokau for collaboration during research work.

References

[1] F. Braghin, F. Cheli, S. Melzi, and F. Resta, "Tyre wear model: validation and sensitivity analysis," *Meccanica*, vol. 41, no. 2, pp. 143–156, 2006.

[2] F. Mancosu, R. Sangalli, F. Cheli, and S. Bruni, "A new mathematical-physical 2D tire model for handling optimization on a vehicle," Tech. Rep. 1999-01-0789, The Society of Automotive Engineers, 1999.

[3] Z.-X. Yu, H.-F. Tan, X.-W. Du, and L. Sun, "A simple analysis method for contact deformation of rolling tire," *Vehicle System Dynamics*, vol. 36, no. 6, pp. 435–443, 2001.

[4] J. Deur, J. Asgari, and D. Hrovat, "A 3D brush-type dynamic tire friction model," *Vehicle System Dynamics*, vol. 42, no. 3, pp. 133–173, 2004.

[5] W. Hall, J. T. Mottram, and R. P. Jones, "Finite element simulation of a rolling automobile tyre to understand its transient macroscopic behaviour," *Proceedings of the Institution of Mechanical Engineers, Part D*, vol. 218, no. 12, pp. 1393–1408, 2004.

[6] J. Pelc, "Static three-dimensional modelling of pneumatic tyres using the technique of element overlaying," *Proceedings of the Institution of Mechanical Engineers, Part D*, vol. 216, no. 9, pp. 709–716, 2002.

[7] N. Miyashita, T. Kawazura, and K. Kabe, "Analytical model of μ-S curve using generalized skewed-parabola," *JSAE Review*, vol. 24, no. 1, pp. 87–92, 2003.

[8] C. Lee, K. Hedrick, and K. Yi, "Real-time slip-based estimation of maximum tire-road friction coefficient," *IEEE/ASME Transactions on Mechatronics*, vol. 9, no. 2, pp. 454–458, 2004.

[9] D. Guan, L. H. Yam, A. Zhang, and J. Shang, "Modeling of tire rolling properties by using experimental modal parameters," Tech. Rep. 2000-01-0361, The Society of Automotive Engineers, 2000.

[10] L. Netsch, Y. Ito, B. Schick, A. Kraus, and M. Berkmüller, "T^{3}M—TÜV Tire temperature method—a breakthrough methodology for evaluating tire robustness, performance and wear," in *Proceedings of 31st FISITA World Automotive Congress*, JSAE, Yokohama, Japan, October 2006, paper F2006V094.

[11] B. N. J. Persson, U. Tartaglino, O. Albohr, and E. Tosatti, "Sealing is at the origin of rubber slipping on wet roads," *Nature Materials*, vol. 3, no. 12, pp. 882–885, 2004.

[12] U. Sandberg and J. A. Ejsmont, *Tire/Road Noise Reference Book*, Harg, Kisa, Sweden, 2003.
[13] A. J. Tuononen, "Optical position detection to measure tyre carcass deflections," *Vehicle System Dynamics*, vol. 46, no. 6, pp. 471–481, 2008.
[14] R. H. Smith, *Analyzing Friction in the Design of Rubber Products and Their Paired Surfaces*, CRC press, Boca Raton, Fla, USA, 2008.
[15] Y. Hu, *Überarbeitung und erweiterung des praktikum-sprüfplatzes zur bestimmung von reifeneigenschaften*, Project Work thesis, Automotive Engineering Department, Ilmenau University of Technology, Ilmenau, Germany, 2007.
[16] V. Ivanov and K. Augsburg, "Assessment of tire contact properties by nondestructive analysis. Part 1. The contact length in the region of adhesion at slow rolling velocities," *Journal of Friction and Wear*, vol. 29, no. 5, pp. 362–368, 2008.
[17] V. Ivanov, K. Augsburg, and B. N. Shyrokau, "Evaluation of tire contact properties using nondestructive testing. Part 2: experimental determination and fuzzy model of the contact parch in the static state," *Journal of Friction and Wear*, vol. 29, no. 6, pp. 448–454, 2008.
[18] National Instruments, NI Vision, "IMAQ Vision Concepts Manual," January 2005.
[19] I. V. Kragelski and N. M. Mikhin, *Friction Units of Machines: Reference Book*, Mashinostroenie, Moscow, Russia, 1984.
[20] V. Boutylin, J. Lepeshko, and V. Ivanov, "About interrelation between the tire grip properties and the wheel sliding," Tech. Rep. 2001-01-3338, The Society of Automotive Engineers, 2001.